nature microbiology

LETTERS

https://doi.org/10.1038/s41564-019-0425-6

Basal expression of interferon regulatory factor 1 drives intrinsic hepatocyte resistance to multiple RNA viruses

Daisuke Yamane[1,2,3,4*], Hui Feng[1,2,3], Efraín E. Rivera-Serrano[1,2,3], Sara R. Selitsky[1], Asuka Hirai-Yuki[1,2,3,5], Anshuman Das[1,2,3], Kevin L. McKnight[1,2,3], Ichiro Misumi[6,7], Lucinda Hensley[1,2,3], William Lovell[1,2,3], Olga González-López[1,2,3], Ryosuke Suzuki[8], Mami Matsuda[8], Hiroki Nakanishi[9], Takayo Ohto-Nakanishi[10], Takayuki Hishiki[4], Eliane Wauthier[1,11], Tsunekazu Oikawa[1,11,12], Kouichi Morita[13], Lola M. Reid[1,11], Praveen Sethupathy[1,14], Michinori Kohara[4], Jason K. Whitmire[1,6,7] and Stanley M. Lemon[1,2,3*]

Current models of cell-intrinsic immunity to RNA viruses centre on virus-triggered inducible antiviral responses initiated by RIG-I-like receptors or Toll-like receptors that sense pathogen-associated molecular patterns, and signal downstream through interferon regulatory factors (IRFs), transcription factors that induce synthesis of type I and type III interferons[1]. RNA viruses have evolved sophisticated strategies to disrupt these signalling pathways and evade elimination by cells, attesting to their importance[2]. Less attention has been paid to how IRFs maintain basal levels of protection against viruses. Here, we depleted antiviral factors linked to RIG-I-like receptor and Toll-like receptor signalling to map critical host pathways restricting positive-strand RNA virus replication in immortalized hepatocytes and identified an unexpected role for IRF1. We show that constitutively expressed IRF1 acts independently of mitochondrial antiviral signalling (MAVS) protein, IRF3 and signal transducer and activator of transcription 1 (STAT1)-dependent signalling to provide intrinsic antiviral protection in actinomycin D-treated cells. IRF1 localizes to the nucleus, where it maintains the basal transcription of a suite of antiviral genes that protect against multiple pathogenic RNA viruses, including hepatitis A and C viruses, dengue virus and Zika virus. Our findings reveal an unappreciated layer of hepatocyte-intrinsic immunity to these positive-strand RNA viruses and identify previously unrecognized antiviral effector genes.

To map host antiviral pathways, we studied immortalized adult human hepatocytes. PH5CH8 cells express RIG-I-like receptors (RLRs) and Toll-like receptors (TLRs) similar to hepatocytes in vivo and induce strong interferon (IFN) and pro-inflammatory cytokine responses when infected with RNA viruses[3–5]. We depleted antiviral factors linked to RLRs and TLRs by transducing cells with lentiviral vectors expressing short-hairpin RNAs (shRNAs) (Supplementary Table 1), and assessed the impact on the replication of hepatitis A virus (HAV), a hepatotropic human picornavirus that causes acute inflammatory liver disease[6]. Surprisingly, depleting RLRs (retinoic acid-inducible gene I protein (RIG-I), melanoma differentiation-associated protein 5 (MDA5) and probable ATP-dependent RNA helicase (LGP2)), signalling adaptors (mitochondrial antiviral signalling (MAVS) protein, stimulator of interferon genes protein (STING), myeloid differentiation primary response protein (MyD88) and TIR-domain-containing adapter-inducing interferon-β (TRIF)) and transcription factors (interferon regulatory factor 3 (IRF3) and IRF7) involved in inducible IFN responses, as well as IFN receptors (interferon alpha/beta receptor 1 (IFNAR1) and interferon lambda receptor 1 (IFNLR1)), resulted in only small increases in HAV replication, whereas depleting IRF1 enhanced HAV RNA levels 30-fold (Fig. 1a and Supplementary Fig. 1a–f). We confirmed the marked increase in HAV replication resulting from IRF1 depletion in CRISPR–Cas9-generated PH5CH8 knockout cell pools transduced with different single guide RNAs (sgRNAs) (*IRF1* no. 1 and *IRF1 no.* 2) (Fig. 1b). In contrast, knocking out *IRF3*, or depleting both IRF3 and IRF7, had little effect on replication (Fig. 1b and Supplementary Fig. 2a). Thus, IRF1 is significantly more active than IRF3 in restricting HAV infection in these cells. Genetically deficient *Irf1*$^{-/-}$ mice also shed more HAV in the faeces and had more viral RNA in the liver than either *Irf3*$^{-/-}$ or wild-type mice 7 d after virus challenge, although HAV did not establish persistent infection as it does in *Ifnar1*$^{-/-}$ mice[7] (Fig. 1c and Supplementary Fig. 2b). IRF1 may promote IFN-γ signalling, major histocompatibility complex class I expression and T cell activation in vivo[8,9].

[1]UNC Lineberger Comprehensive Cancer Center, Chapel Hill, NC, USA. [2]Department of Microbiology & Immunology, The University of North Carolina at Chapel Hill, Chapel Hill, NC, USA. [3]Department of Medicine, The University of North Carolina at Chapel Hill, Chapel Hill, NC, USA. [4]Department of Microbiology and Cell Biology, Tokyo Metropolitan Institute of Medical Science, Setagaya-ku, Tokyo, Japan. [5]Division of Experimental Animal Research, National Institute of Infectious Diseases, Tokyo, Japan. [6]Department of Microbiology, The University of North Carolina at Chapel Hill, Chapel Hill, NC, USA. [7]Department of Immunology and Genetics, The University of North Carolina at Chapel Hill, Chapel Hill, NC, USA. [8]Department of Virology II, National Institute of Infectious Diseases, Shinjuku-ku, Tokyo, Japan. [9]Research Center for Biosignaling, Akita University,, Akita, Japan. [10]Lipidome Lab Co., Ltd,, Akita, Japan. [11]Department of Cell Biology and Physiology Program in Molecular Biology and Biotechnology, University of North Carolina School of Medicine, Chapel Hill, NC, USA. [12]Division of Gastroenterology and Hepatology, Depertment of Internal Medicine, Jikei University School of Medicine, Minato-ku, Tokyo, Japan. [13]Department of Virology, Institute of Tropical Medicine, Nagasaki University, Nagasaki, Japan. [14]Department of Biomedical Sciences, College of Veterinary Medicine, Cornell University, Ithaca, NY, USA. *e-mail: yamane-ds@igakuken.or.jp; smlemon@med.unc.edu

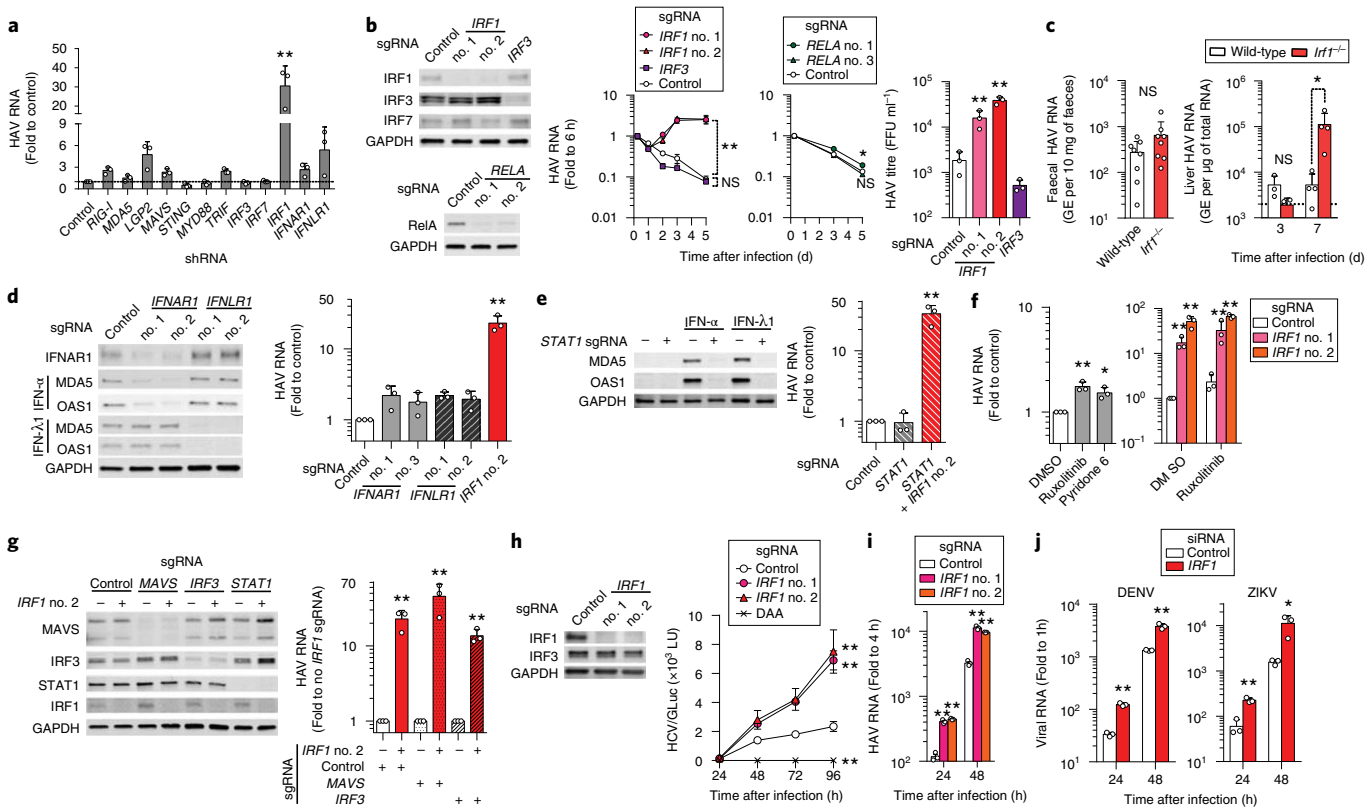

Fig. 1 | IRF1 restricts RNA virus infections in hepatocytes. a, Intracellular HAV RNA 5 d post-inoculation in PH5CH8 cells transduced with lentivirus expressing shRNAs targeting different genes. $^{**}P < 0.01$ versus control (two-way ANOVA with Dunnett's multiple comparisons test). **b**, Kinetics of HAV RNA replication over 5 d in PH5CH8 cells expressing *IRF1* versus *IRF3* versus *RELA* sgRNAs. $^{*}P < 0.05$, $^{**}P < 0.01$ versus control (two-way ANOVA with Dunnett's multiple comparisons test). Immunoblots of IRF1, IRF3, IRF7 and RelA in the knockout cells are shown on the left. Viral titres on 5 d post-inoculation are shown on the right. $^{**}P < 0.01$ versus control (one-way ANOVA with Dunnett's multiple comparisons test). GAPDH, glyceraldehyde-3-phosphate dehydrogenase. **c**, Faecal HAV shedding on days 5 and 7 post-inoculation (left, data are pooled from two different time points) and intrahepatic HAV RNA on days 3 and 7 (right, each symbol = one animal) in wild-type versus *Irf1*$^{-/-}$ C57BL/6 mice. $^{*}P < 0.05$ versus wild-type (two-sided unpaired Mann–Whitney *U*-test). GE, genome equivalent. **d**, HAV RNA 5 d post-inoculation in PH5CH8 cells expressing *IFNAR1* or *IFNLR1* sgRNAs versus *IRF1* sgRNA. Immunoblots of IFNAR1 and ISGs (MDA5 and OAS1) induced either by recombinant IFN-α (100 U ml^{-1} for 24 h) or IFN-λ (10 ng ml^{-1}) in these knockout cells are shown on the left. $^{**}P < 0.01$ versus control (one-way ANOVA with Dunnett's multiple comparisons test). **e**, HAV RNA 5 d post-inoculation in PH5CH8 cells expressing *STAT1* sgRNA and both *STAT1* and *IRF1* sgRNAs (right). $^{**}P < 0.01$ versus control (one-way ANOVA with Dunnett's multiple comparisons test). Immunoblots showing the absence of ISG expression in response to type I and type III IFNs (left). **f**, HAV RNA 5 d post-inoculation in PH5CH8 cells in the continued presence of Jak inhibitors, 3 μM ruxolitinib or 0.3 μM pyridone 6 (left). $^{*}P < 0.05$, $^{**}P < 0.01$ versus control (one-way ANOVA with Dunnett's multiple comparisons test or two-sided Student's *t*-test). Knocking out *IRF1* enhanced HAV replication in the presence of ruxolitinib (right). $^{*}P < 0.05$, $^{**}P < 0.01$ versus control (two-sided unpaired Student's *t*-test). **g**, Effect of double-knockout of *IRF1* in the absence of MAVS or IRF3 expression on HAV replication. Relative HAV RNA levels 5 d post-inoculation, normalized to those without *IRF1* sgRNA were set to 1 (right). Immunoblots are shown on the left. $^{**}P < 0.01$ versus control (two-sided unpaired Student's *t*-test). **h**, Immunoblots of IRF1 in control and *IRF1* knockout Huh-7.5 cells (left). GLuc secreted by Huh-7.5 cells infected with the JFH1-QL/GLuc virus (10^{3} FFU ml^{-1}) over the ensuing 96 h (right). $^{**}P < 0.01$ versus control (two-way ANOVA with Dunnett's multiple comparisons test). **i**, HAV RNA levels in *IRF1* sgRNA-expressing versus control Huh-7.5 cells infected at an MOI of 1 over the ensuing 48 h. $^{**}P < 0.01$ versus control (two-sided unpaired Student's *t*-test). **j**, DENV and ZIKV RNA levels in *IRF1* versus control siRNA-transfected Huh-7.5 cells infected at an MOI of 1 over the ensuing 48 h. $^{*}P < 0.05$, $^{**}P < 0.01$ versus control (two-sided unpaired Student's *t*-test). Data are shown as the mean ± s.d. from three independent experiments (**a**,**b**,**d**–**h**,**j**) or from three technical replicates representative of two independent experiments (**c**,**i**). The precise *P* values are shown in Supplementary Table 9.

Such effects are unlikely to cause enhancement of HAV replication in *Irf1*$^{-/-}$ mice, as previous studies have shown that neither IFN-γ receptor knockout nor the absence of functional T cells renders C57BL/6 mice permissive for infection[7]. Taken collectively, these results suggest that IRF1 restricts viral replication in hepatocytes.

IRF1 is known to induce type I IFN gene expression[10], mediate type III IFN expression downstream of peroxisomal MAVS protein[11] and exert broad antiviral effector activity[12]. However, knocking out receptors for type I or III IFN (*IFNAR1* and *IFNLR1*) enhanced HAV infection less than threefold (Fig. 1d). Moreover, knocking out signal transducer and activator of transcription 1 (*STAT1*), thereby abolishing both type I and type III IFN signalling (Fig. 1e, left panel), caused no increase in HAV replication, whereas additionally knocking out *IRF1* increased replication over 20-fold (Fig. 1e, right panel). Similarly, pharmacological inhibition of Janus kinases (Jak-1/2), key components of IFN-induced Jak/STAT signalling, enhanced viral replication only twofold and failed to blunt increases in replication caused by *IRF1* knockout (Fig. 1f). Collectively, these data show IRF1 restricts HAV replication independently of IFN signalling.

IRF1 expression is regulated in an nuclear factor kappa-light-chain-enhancer of activated B cells (NF-κB)-dependent manner

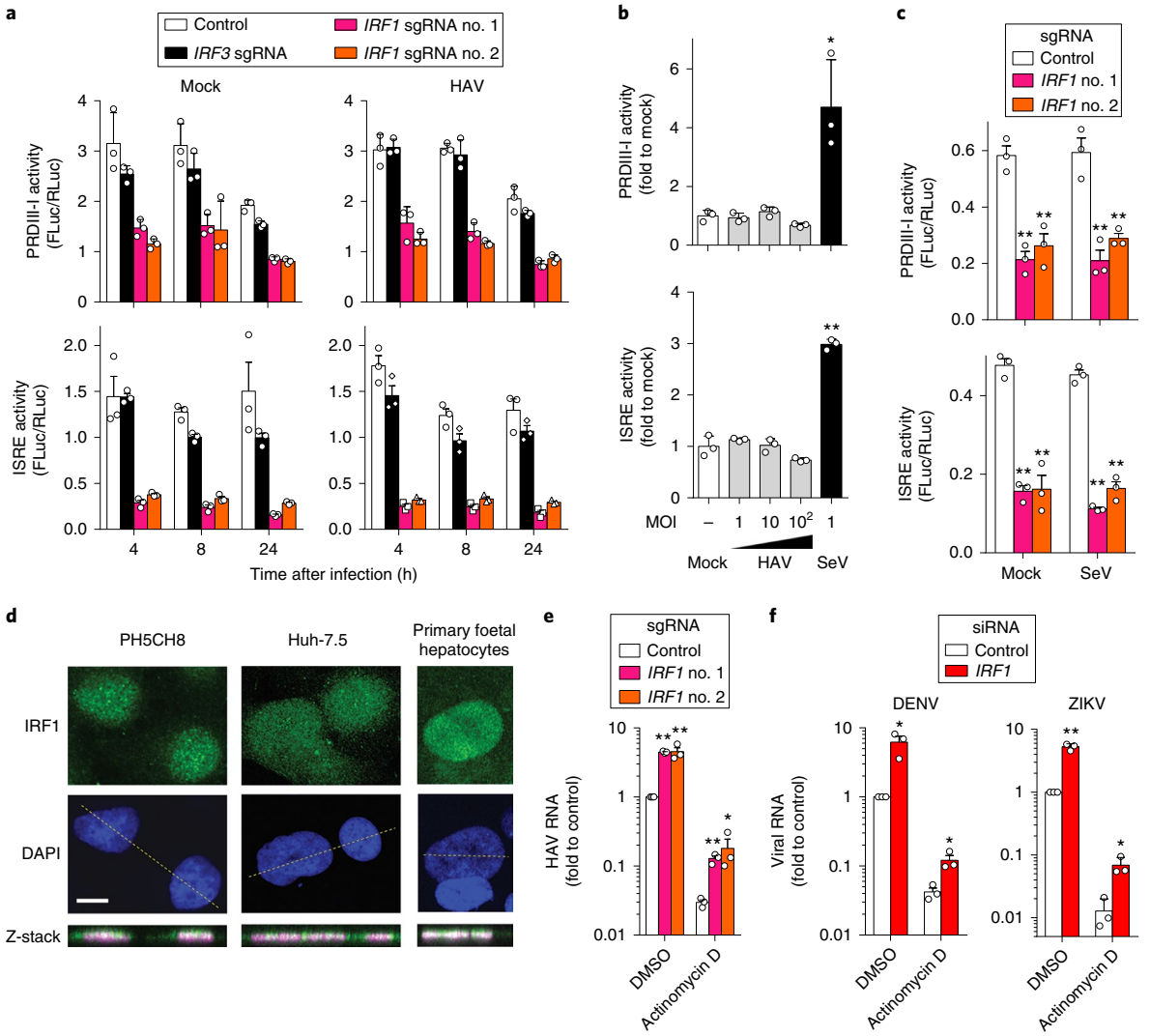

Fig. 2 | IRF1 constitutively activates basal transcription of PRDIII-I- and ISRE-dependent antiviral genes. a, Dual luciferase reporter analysis of 4×PRDIII-I-Luc (top panels) and ISRE-Luc (bottom panels) activities in mock- (left panels) and HAV-infected (right panels) PH5CH8 cells. The promoter activities in *IRF1*-sgRNA (nos. 1 and 2) versus control or *IRF3* sgRNA-expressing cells differed significantly ($P < 0.01$, two-way ANOVA with Dunnett's multiple comparisons test). **b**, Dose–response analysis of PRDIII-I (top) and ISRE (bottom) activities in HAV- and SeV-infected, wild-type PH5CH8 cells at the indicated MOI. $^{*}P < 0.05$, $^{**}P < 0.01$ versus mock (one-way ANOVA with Dunnett's multiple comparisons test). **c**, Dual luciferase reporter analysis of 4×PRDIII-I-Luc (top) and ISRE-Luc (bottom) activity in mock-infected Huh-7.5 cells. Note that SeV does not activate these promoters in Huh-7.5 cells. $^{**}P < 0.01$ versus control (two-way ANOVA with Dunnett's multiple comparisons test). **d**, Nuclear localization of IRF1 in two different hepatic cell lines and primary human foetal hepatocytes. Data are representative of two independent experiments. Scale bar, 20 μm. **e**, HAV RNA at 24 h post-inoculation in Huh-7.5 cells expressing *IRF1* sgRNA pretreated with actinomycin D (5 μg ml^{-1}) for 30 min before infection. $^{*}P < 0.05$, $^{**}P < 0.01$ versus control (two-sided unpaired Student's *t*-test). **f**, DENV RNA at 18 h post-inoculation or ZIKV RNA at 24 h post-inoculation in IRF1-depleted Huh-7.5 cells pretreated with actinomycin D (5 μg ml^{-1}) for 30 min before infection. $^{*}P < 0.05$, $^{**}P < 0.01$ versus control (two-sided unpaired Student's *t*-test). Data are shown as the mean ± s.d. from three technical replicates representative of two independent experiments (**a**–**d**) or from three independent experiments (**e**,**f**). The precise *P* values are shown in Supplementary Table 9.

by RLR-mediated activation of the adaptor protein MAVS[5,11,13]. However, knocking out RELA proto-oncogene, NF-κB subunit (*RELA*) did not enhance HAV replication (Fig. 1b), nor did prior *MAVS* (or *IRF3*) knockout lessen the increases resulting from *IRF1* knockout (Fig. 1g). Moreover, *IRF1* knockout did not diminish Sendai virus (SeV)-induced IFN-β promoter activity or IFN-stimulated gene (ISG) expression, whereas these RIG-I-dependent responses were impaired in knockout *IRF3*-sgRNA cells (Supplementary Fig. 2c). Similarly, antiviral responses triggered by MAVS overexpression required IRF3 but not IRF1 (Supplementary Fig. 2d). Thus, IRF1 restricts HAV infection independently of RelA and MAVS signalling.

Whereas only *IRF1* knockout enhanced infection with cell-free HAV (Fig. 1b), knocking out either *IRF1* or *IRF3* enhanced replication of electroporated synthetic HAV RNA (Supplementary Fig. 2e). *IRF1* and *IRF3* knockout resulted in equivalent and additive increases up to 3 d post-transfection, but *IRF1* knockout (both *IRF1*-sgRNA no. 1 and *IRF1-sgRNA* no. 2) had a greater effect at 5 d when de novo infection with newly replicated virus accounted for continuing increases in RNA abundance. Electroporated RNA, but not cell-free virus infection, also stimulated IRF3-dependent ISG expression (Supplementary Fig. 2f), probably reflecting greater immediate cytoplasmic delivery of viral RNA. Collectively, these results show that IRF1 and IRF3 act non-redundantly, with IRF1

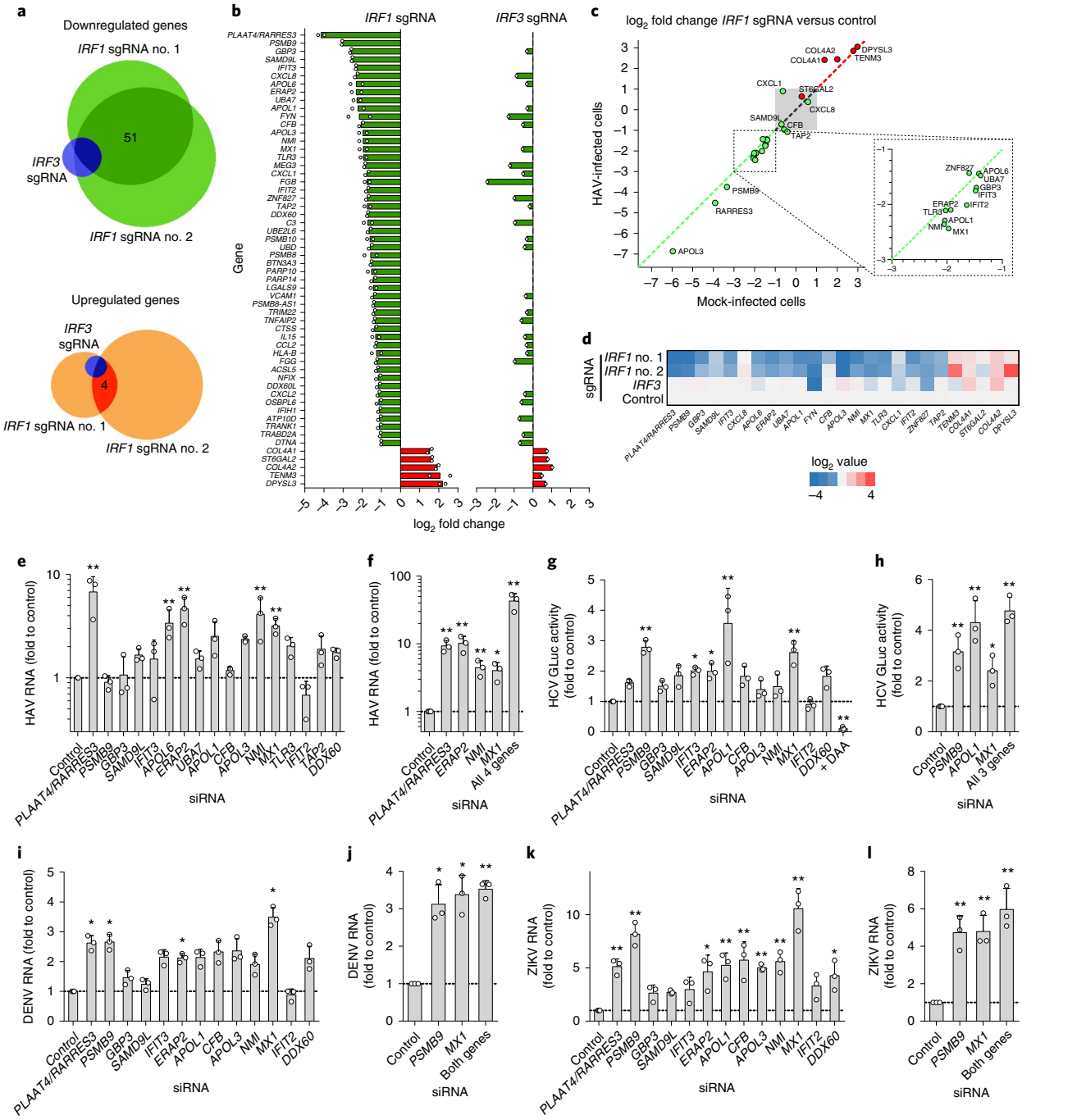

Fig. 3 | Shared and distinct antiviral activities of IRF1 effector genes identified by high-throughput RNA-seq. a, Venn diagram showing the numbers of genes with expression changes of ≥twofold for each knockout. **b**, List of genes reduced >twofold in *IRF1* sgRNA-expressing cells, compared with *IRF3* sgRNA-expressing cells. The values shown are the means of fold changes of genes expressed in cells transduced with two independent *IRF1* sgRNAs (left) or an *IRF3* sgRNA (right). See Supplementary Tables 5–7 for more details. **c**, Validation of RNA-seq results by RT–qPCR assays of RNA extracted from non-infected versus HAV-infected PH5CH8 cells. The scatter plots show the ratio of abundance of the indicated genes between *IRF1* versus control sgRNA-expressing PH5CH8 cells in HAV-infected (*y* axis) and mock-infected cells (*x* axis). **d**, Heatmap showing the relative abundance of the indicated genes in non-infected PH5CH8 cells determined by RT–qPCR. **e**, Relative HAV RNA abundance 5 d post-inoculation of PH5CH8 cells transfected with siRNA targeting different IRF1 effector genes. $^{**}P < 0.01$ versus control. **f**, Independent validation of the siRNA results and the combination of four siRNAs. $^{*}P < 0.05$, $^{**}P < 0.01$ versus control. **g**, Relative GLuc activity 3 d post-inoculation of HCV-infected Huh-7.5 cells. $^{*}P < 0.05$, $^{**}P < 0.01$ versus control. **h**, Independent validation of the siRNA results and combination of three siRNAs. $^{*}P < 0.05$, $^{**}P < 0.01$ versus control. **i**, Relative DENV RNA 24 h post-inoculation of infected Huh-7.5 cells. $^{*}P < 0.05$ versus control. **j**, Independent validation of the siRNA results and combination of two siRNAs. $^{*}P < 0.05$, $^{**}P < 0.01$ versus control. **k**, ZIKV RNA abundance 24 h post-inoculation of infected Huh-7.5 cells. $^{*}P < 0.05$, $^{**}P < 0.01$ versus control. **l**, Independent validation of the siRNA results and combination of two siRNAs. $^{**}P < 0.01$ versus control. Data are shown as the mean ± s.d. from three independent experiments (**e**–**g**,**i**–**l**) or from three technical replicates representative of two independent experiments (**h**). *P* values were derived using a one-way ANOVA with Dunnett's multiple comparisons test (**e**,**g**,**i**–**l**) or a two-sided unpaired Student's *t*-test (**f**,**h**). The precise *P* values are shown in Supplementary Table 9.

mediating protection against an early, post-entry step in HAV infection that does not elicit detectable IRF3 responses.

IRF1 depletion also promoted replication of HAV, as well as hepatitis C virus (HCV), dengue virus (DENV) and Zika virus (ZIKV), all members of the Flaviviridae family in Huh-7.5 cells, a human hepatoma cell line deficient in RIG-I and TLR3 signalling[3,14] (Fig. 1h–j and Supplementary Fig. 3a). The absence of IFN responses in Huh-7.5 cells is supported by a lack of enhancement of HCV, HAV or DENV replication following ruxolitinib treatment (Supplementary Fig. 3b). IRF1 thus restricts replication of multiple pathogenic positive-strand RNA viruses in hepatocyte-derived cells. IRF1 depletion enhanced replication of transfected HCV RNA more than depleting IRF3, RLRs, MAVS or IFN receptors in PH5CH8 cells (Supplementary Fig. 4a–e); as with HAV, its impact on HCV was not reduced by pharmacological blockade of IFN signalling (Supplementary Fig. 4f).

IRF1 protein abundance was not increased in HAV-infected PH5CH8 cells (Supplementary Fig. 5a), and high multiplicity infection failed to stimulate IRF1-responsive PRDIII-I and IFN-stimulated response element (ISRE) promoter elements (Fig. 2a,b)[15–17]. However, knocking out *IRF1* markedly reduced the basal activities of these promoters in both PH5CH8 and Huh-7.5 cells (Fig. 2a,c), whereas ruxolitinib inhibition of Jak/STAT signalling did not (Supplementary Fig. 5b). Collectively, these results suggest that basal expression of IRF1 provides intrinsic antiviral protection by maintaining constitutive transcription of antiviral genes, which is consistent with the nuclear localization of IRF1 in uninfected PH5CH8 and Huh-7.5 cells, and primary human foetal hepatocytes (Fig. 2d and Supplementary Fig. 5c). Further supporting this hypothesis, IRF1 depletion boosted replication of HAV, DENV and ZIKV in the absence of cellular transcription in actinomycin D-treated Huh-7.5 cells (Fig. 2e,f and Supplementary Fig. 5d).

To identify specific IRF1-regulated antiviral effectors, we compared the transcriptomes of HAV-infected *IRF1* and *IRF3* knockout PH5CH8 cells (Fig. 3a). Changes in transcript abundance from cells expressing control sgRNA were highly congruent in two independent *IRF1* knockout cell lines, with 51 genes commonly downregulated > twofold (Spearman's $r = 0.814$; Fig. 3a,b, Supplementary Fig. 6a,b and Supplementary Table 5). Notably, these genes included known viral sensors (*IFIH1*, *TLR3*), IFN-regulated antiviral effectors (*MX1*, *IFIT2*, *IFIT3*), chemotactic factors (*CCL2, CXCL1, CXCL2, CXCL8*) and components of the immunoproteasome (*PSMB8*, proteasome subunit beta 9 (*PSMB9*) and *PSMB10*), in addition to multiple genes with no previously recognized antiviral function (Supplementary Tables 5 and 6). Only three of these transcripts were downregulated > twofold in *IRF3*-sgRNA cells (Fig. 3b and Supplementary Table 7).

We focused on the 18 genes most downregulated in *IRF1* knockout cells. With the exception of *CXCL8*, reverse transcription quantitative PCR (RT–qPCR) confirmed > twofold reductions in basal expression of each in *IRF1* knockout PH5CH8 cells (Fig. 3c,d). Basal proteasome subunit beta type-9 (PSMB9), N-myc-interactor (NMI) and TLR3 protein abundances were also reduced, and TLR3 sensing of poly(I:C) lost after *IRF1* knockout (Supplementary Fig. 7a,b). Importantly, the impact of IRF1 knockout on transcript levels was equivalent in HAV-infected and uninfected cells (Spearman $r = 0.944–0.963$, $P < 0.001$; Fig. 3c). Thus, IRF1 restricts HAV replication by driving constitutive, basal transcription of antiviral effector genes. Importantly, each of these genes is expressed basally in primary human hepatocytes and hepatoblasts[18] (Supplementary Fig. 7c).

Transfecting PH5CH8 cells with small interfering RNA (siRNA) pools (Supplementary Table 4 and Supplementary Fig. 7e) targeting phospholipase A and acyltransferase 4 (*PLAAT4*/*RARRES3*), apolipoprotein L6 (*APOL6*), endoplasmic reticulum aminopeptidase 2 (*ERAP2*), N-myc and STAT interactor (*NMI*) or MX dynamin like GTPase 1 (*MX1*) enhanced HAV replication > threefold (Fig. 3e). Good correlation between knockdown efficiency of individual siRNAs and replication enhancement validated these results for all but *APOL6* (Supplementary Fig. 7f). Importantly, simultaneously silencing *PLAAT4*/*RARRES3*, *ERAP2*, *NMI* and *MX1* boosted replication around 40-fold (Fig. 3f), recapitulating the phenotype of *IRF1* knockout cells (Fig. 1b). Similar experiments in Huh-7.5 cells demonstrated that different subsets of basally IRF1-regulated genes restrict replication of HCV (*PSMB9*, *APOL1* and *MX1*), and DENV and ZIKV (*PSMB9* and *MX1*) (Fig. 3g–l). Overexpression confirmed the antiviral activities of PSMB9 against HCV and the flaviviruses, as well as the HCV-specific antiviral activity of apolipoprotein L1 (APOL1; Supplementary Fig. 7g–i). Thus, IRF1 basally regulates suites of genes that, in various combinations, restrict replication of different positive-strand RNA viruses. Silencing these genes did not affect cell proliferation (Supplementary Fig. 7j).

PLAAT4/*RARRES3*, the gene most downregulated by IRF1 knockout and most active in restricting HAV (Fig. 3e,f), encodes a single-pass transmembrane protein with acyl transferase activity[19]. Although shown previously to modestly limit poliovirus replication[12], *PLAAT4*/*RARRES3* is not recognized as an important restriction factor for any virus. IFN-γ induced the accumulation of nuclear IRF1 and restricted HAV replication in an IRF1-dependent manner in Huh-7.5 cells; silencing *PLAAT4*/*RARRES3* partially attenuated this suppressive effect of IFN-γ (Supplementary Figs. 5c and 7k,l). Moreover, expressing catalytically active retinoic acid receptor responder protein 3 (RARRES3) in *IRF1* knockout cells ablated HAV replication, whereas a Cys^{113}-Ser mutant (C113S) lacking acyl transferase activity did not (Fig. 4a). Similar results were obtained in Huh-7.5 cells (Fig. 4a). Although its paralog, PLA2G16 (52% amino acid identity), is a proviral entry factor for several picornaviruses[20], RARRES3 inhibited neither entry nor translation of a nanoluciferase-expressing HAV (HM175/18f-NLuc, 'HAV/NLuc'; Fig. 4b) whereas it blocked replication of a subgenomic RNA replicon (Fig. 4c). Huh-7.5 cells knocked out for *PLAAT4*/*RARRES3* demonstrated enhanced replication of the HAV/NLuc virus (Fig. 4d). Although potent, the antiviral action of RARRES3 was specific to HAV, as overexpression did not restrict replication of HCV, DENV or human rhinovirus 14 (HRV-14) (Supplementary Fig. 8a).

The acyl transferase activity of RARRES3 may exert pleiotropic effects on cellular signalling pathways, including the PI3K/Akt/mTOR axis[21,22]. RARRES3 overexpression induced phosphorylation of p70-$S6K^{Thr\ 389}$ in an acyl transferase-dependent manner, downregulating mTOR by catalysing its phosphorylation at Ser 2448[23,24] and reducing mTOR-dependent phosphorylation of 4E-BP1 at Thr 70 (Fig. 4e,f). Consistent with this, both p70-S6K and mTOR phosphorylation were reduced in *IRF1* knockout cells (Fig. 4g). Pharmacological inhibition of mTOR also inhibited HAV, but not HCV or DENV replication (Fig. 4h,i). Thus, although we cannot exclude additional antiviral actions, RARRES3 probably exerts an antiviral effect by downregulating mTOR. Despite its phospholipase activity[19], overexpressing RARRES3 resulted only in minimal increases in phosphoinositide PI(3,4,5)P3 and no other changes among 211 lipid species (Supplementary Fig. 8b).

These data establish RARRES3 as an important IRF1-regulated HAV restriction factor. Of the other three genes with major restriction activity against HAV (Fig. 3e), only *MX1* is well known for its antiviral activities. *NMI* was suggested previously to promote degradation of IRF7 and to function as a proviral, negative regulator of IFN responses[25]. Endoplasmic reticulum aminopeptidase 2 (ERAP2), an endosomal aminopeptidase, contributes to T cell responses by generating class I human leukocyte antigen-binding peptides, but it has no known cell-intrinsic antiviral activity. Interestingly, we found that PSMB9, a component of the immunoproteasome that is also involved in antigen processing[26], provides basal antiviral protection against HCV and the flaviviruses, DENV and ZIKV (Fig. 3g–l and

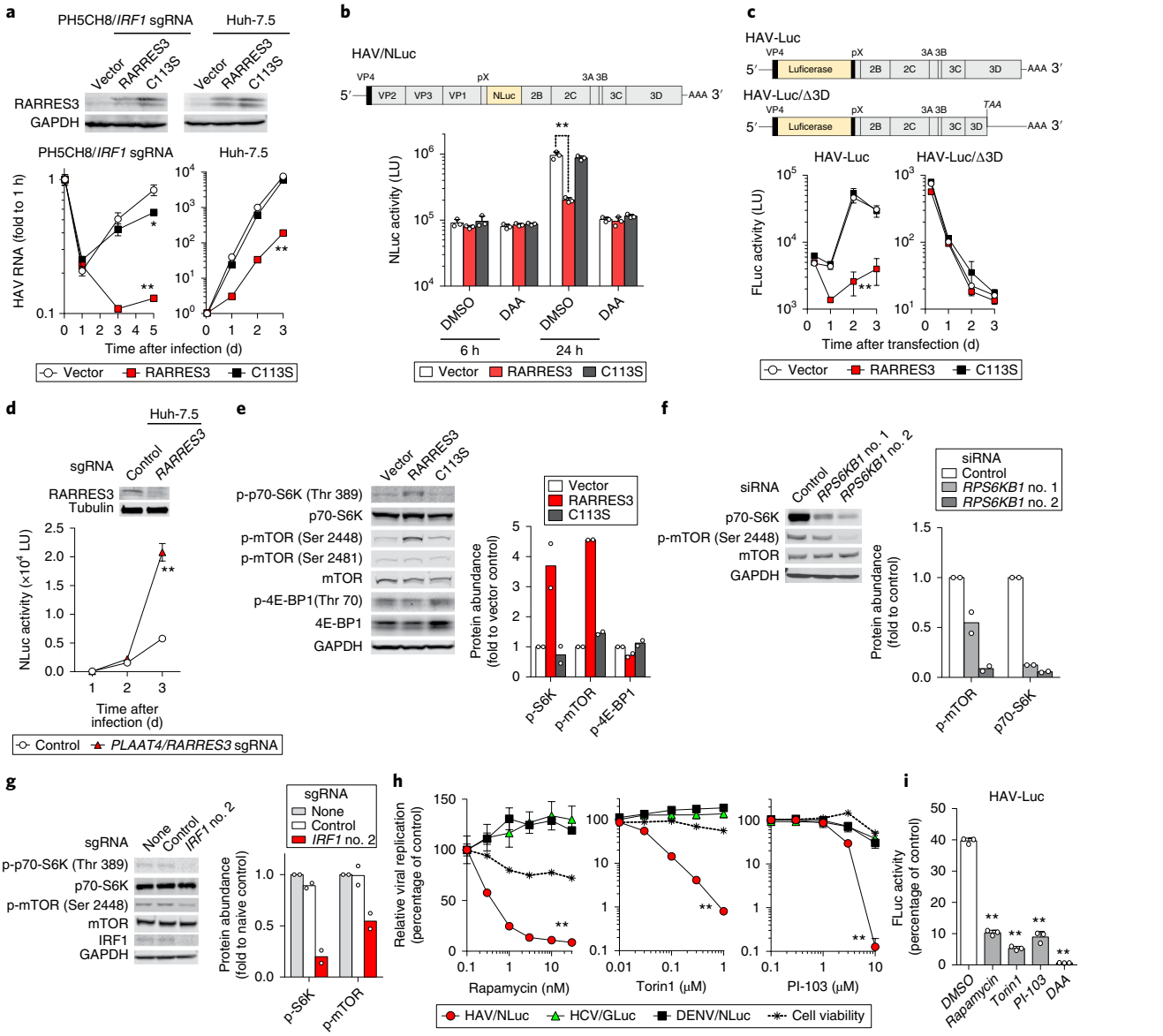

Fig. 4 | IRF1-regulated RARRES3 acyl transferase restricts HAV replication by downregulating mTOR. a, Lentivirus transduction of catalytically active RARRES3 restricts HAV infection in PH5CH8 cells expressing *IRF1* sgRNA no. 2 (left panels) or Huh-7.5 cells (right panels). RARRES3, but not its catalytically inactive RARRES3/C113S mutant, inhibited HAV infection in both cell lines. $^{*}P < 0.05$, $^{**}P < 0.01$ versus vector control (two-way ANOVA with Dunnett's multiple comparisons test). **b**, Huh-7.5 cells stably expressing indicated lentiviral vectors were challenged with HAV carrying NLuc with 30 μM 2′ CMA (direct-acting antiviral (DAA)) or vehicle (dimethylsulfoxide (DMSO)). NLuc activities at the indicated time points post-infection are shown. $^{**}P < 0.01$ (two-way ANOVA with Dunnett's multiple comparisons test). **c**, Transfection of subgenomic HAV-Luc RNA or its replication-incompetent mutant (Δ3D) in Huh-7.5 cells expressing wild-type RARRES3 versus the RARRES3/C113S mutant. $^{**}P < 0.01$ versus vector control (two-way ANOVA with Dunnett's multiple comparisons test). **d**, Infection of HAV/NLuc in Huh-7.5 cells expressing *PLAAT4/RARRES3* sgRNA. Immunoblots are shown on the top. $^{**}P < 0.01$ versus vector control (two-way ANOVA with Dunnett's multiple comparisons test). **e**, Steady-state levels of mTOR-related factors in Huh-7.5 cells stably expressing RARRES3 and RARRES3/C113S. **f**, Immunoblots of P70-S6K siRNA-transfected Huh-7.5/RARRES3 cells. **g**, Phosphorylation of p70-S6K and mTOR in Huh-7.5 cells expressing *IRF1* sgRNA. **h**, Impact of mTOR inhibitors on HAV/NLuc versus HCV/GLuc versus DENV/NLuc replication and cell viability. The inhibitory effects of all these inhibitors on HAV/NLuc versus other reporter viruses differed significantly. $^{**}P < 0.01$ (two-way ANOVA with Dunnett's multiple comparisons test). **i**, Inhibition of transfected subgenomic HAV/NLuc RNA replication in Huh-7.5 cells by three mTOR inhibitors and a DAA (30 μM 2′CMA). $^{**}P < 0.01$ versus DMSO control (one-way ANOVA with Dunnett's multiple comparisons test). Data are shown as the mean ± s.d. from three independent experiments (**b**,**d**,**i**) or from three technical replicates representative of two (**a**,**e**–**h**) or three independent experiments (**c**). The precise *P* values are shown in Supplementary Table 9.

Supplementary Fig. 7h–i). Additional studies are needed, but these results point to potential unrecognized intrinsic antiviral functions of the antigen processing machinery and may help to explain active suppression of the immunoproteasome by many viruses[26,27]. Thus, although many of the basally IRF1-regulated genes we identified have been linked to IFN responses previously, only a minority (for example, *MX1* and *IFIT3*) have well-established direct antiviral function[28].

Our data show differences in the key IRF1-regulated genes that basally restrict replication of various positive-strand RNA viruses (Fig. 3e–l). Differences may also exist between mammalian species, perhaps reflecting evolutionary history with viruses. Mice (*Mus musculus*) are not naturally permissive for HAV infection, due to overwhelming virus control by MAVS and IRF3/IRF7-mediated transcriptional responses[7]. Nonetheless, HAV replication is enhanced in *Irf1*$^{-/-}$ mice early after infection (Fig. 1c), even though orthologues of two of the four IRF1-regulated genes that most restrict HAV replication in human hepatocytes, *PLAAT4*/*RARRES3* and *ERAP2*, do not exist in mice (Fig. 3e,f).

IRF1 has been shown previously to contribute to the basal expression of dozens of IFN-γ inducible pro-inflammatory and antimicrobial genes in macrophages[29], but its crucial role in basally regulating genes that restrict virus replication has not been appreciated. Our data show that the constitutive expression of IRF1 maintains basal transcription of suites of genes, some with no previously known antiviral function, that provide immediate defence against viral invasion of hepatocytes. As IRF1 also mediates early protection against alphaviruses in muscle cells independently of IFNs[30], it may act similarly in non-hepatic tissues. Little attention has been paid previously to this aspect of IRF1-regulated, cell-intrinsic immunity. Further elucidating the mechanisms by which IRF1-regulated restriction factors act to intrinsically limit virus replication may provide fresh directions for host-directed antiviral therapies.

Methods

Cells. Huh-7.5 human hepatoma cells and PH5CH8 immortalized human hepatocytes were mycoplasma-free and cultured in DMEM-high glucose supplemented with 10% foetal bovine serum, 1×penicillin-streptomycin, 1×GlutaMAX-I and 1×MEM non-essential amino acids solution (Thermo Fisher Scientific), as described previously[31,32].

Tissues for processing foetal liver cells were provided by the accredited non-profit corporation Advanced Bioscience Resources and obtained from fetuses between 19 and 21 weeks' gestation during elective terminations of pregnancy. Tissues were collected with written informed consent from all donors and in accordance with the United States Food and Drug Administration's Good Tissue Practices regulations, Code of Federal Regulations Part 1271. Tissue processing, and the isolation and culture of hepatoblasts, were described previously[32]. The use of commercially procured foetal liver cells was determined by the University of North Carolina (UNC) at Chapel Hill Institutional Review Board to be exempt from review.

HAV infectious challenge in genetically modified mice. Mice were bred and housed at UNC-Chapel Hill in accordance with the policies and guidelines of the Institutional Animal Care and Use Committee. C57BL/6, *Ifnar1*$^{-/-}$, *Irf3*$^{-/-}$ and *Irf1*$^{-/-}$ mice were purchased from The Jackson Laboratory. Mice were intravenously inoculated with the indicated virus inocula at 6–10 weeks of age, as described previously[7]. Mice were housed in individual cages for collection of faecal pellets with periodic collection of serum samples. Tissues were collected at necropsy and stored in RNAlater (Thermo Fisher Scientific), or snap-frozen on dry ice and kept at −80 °C until processed for RNA extraction. All experiments involving mice were approved by the UNC-Chapel Hill Institutional Animal Care and Use Committee.

Reagents and antibodies. MicroRNA-122 mimics were synthesized by Dharmacon and transfected by electroporation as miRNA/miRNA* duplexes as described previously[33]. Puromycin, blasticidin and ruxolitinib were purchased from InvivoGen. Pyridone 6 was sourced from EMD Millipore. Recombinant human IFN-λ1 and IFN-α, and actinomycin D were purchased from from Sigma-Aldrich. Recombinant human IFN-γ was obtained from PeproTech. PSI-7977 (Sofosbuvir) was obtained from ChemScene and 2′-C-methyladenosine (2′ CMA) was obtained from Santa Cruz Biotechnology. Cell viability was determined using Cell Counting Kit-8 (Dojindo) on 96-well plates according to the manufacturer's protocol.

Primary antibodies to IRF-1 (D5E4) XP (1:500 dilution, catalogue no. 8478), IRF-7 (D2A1J) (1:500 dilution, catalogue no. 13014), IFIT1 (1:500 dilution, catalogue no. 14769), Stat1 (D1K9Y) (1:500 dilution, catalogue no. 14994), STING (D2P2F) (1:500 dilution, catalogue no. 13647), MyD88 (D80F5) (1:500 dilution, catalogue no. 4283), TLR3 (D10F10) (1:500 dilution, catalogue no. 6961), NF-κB p65 (D14E12) XP (1:500 dilution, catalogue no. 8242), mTOR (7C10) (1:500 dilution, catalogue no. 2983), phospho-mTOR (Ser 2448) (D9C2) XP (1:500 dilution, catalogue no. 5536), phospho-mTOR (Ser 2481) (1:500 dilution, catalogue no. 2974), p70 S6 kinase (49D7) (1:1,000 dilution, catalogue no. 2708), phospho-p70 S6 kinase (Thr 389) (1:1,000 dilution, catalogue no. 9234), 4E-BP1 (53H11) (1:1,000 dilution, catalogue no. 9644) and phospho-4E-BP1 (Thr 70) (1:1,000 dilution, catalogue no. 9455) were obtained from Cell Signaling Technology; IRF-3 (FL-425) (1:200 dilution, catalogue no. sc-9082) and 2′-5′-oligoadenylate synthase 1 (OAS1) (F-3) (1:100 dilution, catalogue no. sc-374656) were obtained from Santa Cruz Biotechnology; anti-DHX58/RLR (1:500, catalogue no. ab67270) was obtained from Abcam; GAPDH monoclonal antibody was obtained from Thermo Fisher Scientific (clone 6C5; 1:10,000 dilution, catalogue no. AM4300) or Wako (clone 5A12; 1:4,000 dilution, catalogue no. 016–25523); RIG-I (clone Alme-1; 1:1,000 dilution, catalogue no. ALX-804–849), Cardif (VISA/IPS-1/MAVS; 1:2,000 dilution, catalogue no. ALX-210–929-C100) and melanoma differentiation-associated protein 5 (1:1,000 dilution, catalogue no. ALX-210–935-C100) were obtained from Enzo Life Sciences; anti-β-actin (clone AC-74; 1:40,000 dilution, catalogue no. A2228), anti-α-tubulin (clone DM1A; 1:15,000 dilution, catalogue no. T6199) and anti-IL28RA (IFNLR1; 1:500 dilution, catalogue no. AV48070) were obtained from Sigma-Aldrich; IFNAR1 (1:2,000 dilution, catalogue no. A304–290A) and NMI (1:4,000 dilution, catalogue no. A300–551A) were obtained from Bethyl Laboratories; and LMP2 (PSMB9; 1:400 dilution, catalogue no. 14544–1-AP), APOL1 (1:500 dilution, catalogue no. 11486-2-AP) and RARRES3 (1:800 dilution, catalogue no. 12065-1-AP) were obtained from Proteintech. IRDye 680 or 800 secondary antibodies, including catalogue no. 926-32211, 926-32212, 926-32214, 926-68020 and 926-68073 (1:12,000), were purchased from LI-COR Biosciences.

Viruses. The high-titre HAV (HM175/18f strain) stock was mycoplasma-free and prepared as described previously[34]. HAV infection was performed at a multiplicity of infection (MOI) of 10. SeV (Cantell strain) was obtained from Charles River Laboratories and was inoculated at 50 U ml^{-1}, unless otherwise indicated. Infection with HCV-carrying *Gaussia* luciferase (GLuc) reporter was described previously[32]. DENV serotype 2 (o1Sa-054 strain) and ZIKV (MR-766 and AB-59 strains) were propagated in Vero, C6/36 or Huh-7.5 cells as described previously[35] and inoculated at an MOI of 1.

HM175/18f-NLuc reporter virus. The pHM175/18f-NLuc plasmid was created using PCR to amplify the NLuc open reading frame using the pNL1.1 plasmid (Promega) as the template and primers containing the triglycine sequence flanked by XbaI and BamHI restriction sites. This PCR product was digested with these enzymes and ligated into a similarly digested pSK-2A-Zeo-2B plasmid[36] to obtain the pSK-2A-NLuc-2B plasmid. This plasmid was further digested with SacI/PflMI to release the entire 2A-NLuc-2B fragment and ligated into a similarly digested HM175/18f parental plasmid[37] to obtain pHM175/18f-NLuc report virus.

DENV/NLuc reporter virus. Plasmids encoding capsid and subgenomic RNA containing NS1-5 region fused with a NanoLuc reporter flanked by 5′ and 3′ untranslated RNAs derived from DENV1 (D1/Hu/Saitama/NIID100/2014 strain) and premembrane and envelope protein derived from DENV2 (o1Sa-054 strain) were transfected into HEK293T cells; infectious virions secreted into the supernatant fluids were collected in accordance with previously described methods[38].

Other plasmids. pJFH1-QL containing the cell culture-adaptive mutation Q221L in the NS3 helicase, pJFH1/GND, pH77S.3, pH77D, pT7-18f, pHAV-Luc and pHAV-LucΔ3D were described previously[32,34,39]. The lentiviral transfer plasmids encoding the IRF1 effector genes (*PLAAT4*/*RARRES3*, *PSMB9* and *APOL1*) were created using PCR to amplify the host genes using complementary DNA derived from PH5CH8 cell total RNA as the template and primers flanked by XbaI and PstI or NheI restriction sites. The PCR products were digested with these enzymes and ligated into a similarly digested pCSII-EF-MCSII plasmid to obtain pCSII-EF-RARRES3, -PSMB9 and -APOL1. A point mutation in pCSII-EF-RARRES3/C113S was introduced by primer-directed mutagenesis of the sequence spanning the XbaI and PstI sites. The firefly luciferase reporter vectors, including pIFN-β-Luc and p4×PRDIII-I-Luc, as well as the *Renilla* luciferase control reporter vector pRL-TK were described previously[3,31].

Viral RNA transcription and transfection. In vitro transcription of HAV or HCV RNA was carried out using T7 RiboMAX Express Large Scale RNA Production System (Promega), following the manufacturer's protocol. Transfection of viral RNA was performed in a Gene Pulser Xcell Total System (Bio-Rad Laboratories) as previously described[33] or using a *Trans*IT-mRNA Transfection Kit (Mirus) for HAV-Luc RNA as described previously[32].

Lentivirus production and transduction. For shRNA lentivirus production, shRNA plasmids obtained from Sigma-Aldrich (listed in Supplementary Table 1) were co-transfected with MISSION Lentiviral Packaging Mix (catalogue no. SHP001; Sigma-Aldrich) into 293FT cells; the supernatant fluids collected at 48 and 72 h were filtered through a 0.22 μm syringe filter. Production of sgRNA CRISPR–Cas9 lentivirus was carried out by co-transfecting the sgRNA-expressing vectors listed in Supplementary Table 2 and 3rd Generation Packaging System Mix (catalogue no. LV053; abm). Lentiviral transduction was performed by supplementation of 8 μg ml^{-1} polybrene, followed by antibiotic selection with 6 μg ml^{-1} puromycin for single knockout derivatives, or 6 μg ml^{-1} puromycin plus

5 μg ml^{-1} blasticidin for double-knockout derivatives. We used antibiotic-resistant bulk cell populations for the experiments to avoid clonal biases.

RNA extraction and RT–qPCR. Total RNA extraction was performed with the RNeasy Mini Kit (QIAGEN). Detection of HAV genome RNA was carried out by a two-step RT–qPCR analysis with the SuperScript III First-Strand Synthesis System (Thermo Fisher Scientific) and iTaq Universal SYBR Green Supermix (Bio-Rad Laboratories) or alternatively the Thunderbird SYBR qPCR Mix (TOYOBO) using the specific primers 5′-GGTAGGCTACGGGTGAAAC-3′ and 5′-AACAACTCACCAATATCCGC-3′. HCV RNA levels were determined as described previously[32]. Quantification of the IRF1 target genes was performed with the primer pairs listed in Supplementary Table 3. DENV and ZIKV RNA levels were quantified using specific primer pairs that targeted the DENV genome RNA, 5′-ACACCACAGAGTTCCATTACAGA-3′ and 5′-CATCTCATTAAAGTCGA GGCC-3′, or the ZIKV genome RNA, 5′-AARTACACATACCARAACAAAGTG GT-3′ and 5′- TCCRCTCCCYCTYTGGTCTTG-3′, respectively, using RNA-direct SYBR Green Realtime PCR Master Mix (TOYOBO).

Phospholipid preparation. The methods for comprehensive phospholipid analysis were described previously[40,41]. Briefly, total phospholipids were extracted from the cell culture with the Bligh–Dyer method. An aliquot of the lower/organic phase was evaporated to dryness under N_2; the residue was then dissolved in methanol for liquid chromatography–tandem mass spectrometry (LC/MS/MS) measurements of phosphatidylcholine and phosphatidylethanolamine. To analyse phosphatidic acid, phosphatidylserine, phosphatidylinositol and PI-phosphate, -bisphosphate and -trisphosphate, another aliquot of the same lipid extract was added with an equal volume of methanol before being loaded onto a diethylaminoethyl cellulose column (Santa Cruz Biotechnology) pre-equilibrated with chloroform. After successive washes with chloroform/methanol (1:1, v/v), the acidic phospholipids were eluted with chloroform/methanol/HCl/water (12:12:1:1, v/v), followed by evaporation to dryness to give a residue that was resolved in methanol. The resultant fraction was subjected to a methylation reaction with trimethylsilyldiazomethane before LC/MS/MS analysis[42].

Mass spectrometry analyses. LC-electrospray ionization-MS/MS analysis was performed with an UltiMate 3000 LC System (Thermo Fisher Scientific) equipped with an HTC PAL Autosampler (CTC Analytics). A 10 μl aliquot of the lipid sample was injected and the lipids were separated on a Waters X Bridge C18 column (3.5 μm, 150 mm × 1.0 mm internal diameter) at room temperature (25 °C) using a gradient solvent system as follows: mobile phase A (isopropanol/methanol/water (5:1:4, v/v/v) supplemented with 5 mM ammonium formate and 0.05% ammonium hydroxide)/mobile phase B (isopropanol supplemented with 5 mM ammonium formate and 0.05% ammonium hydroxide) ratios of 70/30% (0 min), 50/50% (2 min), 20/80% (13 min), 5/95% (15–30 min), 95/5% (31–35 min) and 70/30% (35–45 min). Flow rate was 20 μl min^{-1}. Phospholipid species were measured using selected reaction monitoring in positive ion mode with a triple-stage quadrupole mass spectrometer (TSQ Vantage AM; Thermo Fisher Scientific). The characteristic fragments of individual phospholipids were detected by the product ion scan (MS/MS mode). Chromatographic peak areas were used for comparative quantitation of each molecular species (for example, 38:6, 40:6) in a given class of phospholipids (for example, phosphatidic acid, phosphatidylcholine).

Immunoblots. Western blotting was performed using standard methods. The Odyssey CLx Infrared Imaging System (LI-COR Biosciences) was used for visualization.

RNA interference. The siRNA pools listed in Supplementary Table 4 were obtained from Dharmacon or Thermo Fisher Scientific and transfected into cells using siLentfect Lipid Reagent for RNAi (Bio-Rad Laboratories) or Lipofectamine RNAiMAX Transfection Reagent (Thermo Fisher Scientific) according to the manufacturer's protocol.

Luciferase assay. GLuc analysis of HCV replication and a dual luciferase assay to analyse transcriptional induction were performed as described previously[31,32]. NanoLuc activity was measured using Nano-Glo Luciferase Assay System (Promega), following the manufacture's protocol. For the virus replication assays, the medium was replaced with fresh medium containing chemical inhibitors 1 h after inoculation.

RNA-sequencing (RNA-seq). RNA purity was assessed with a NanoDrop 2000 spectrophotometer (Thermo Fisher Scientific) and integrity was determined with an 2100 Bioanalyzer Instrument (Agilent Technologies). RNA integrity and sequencing quality were comparable for all samples. Sequencing was performed on an HiSeq 2000 platform (Illumina). RNA sequences were aligned to hg38 using STAR v.2.4.2a[43], genes were quantified using SalmonBeta-0.4.2[44] and differential expression was determined with DESeq2[45]. Gene ontology enrichment analysis was performed with DAVID 6.8.

Confocal laser-scanning microscopy. Cells grown on an 8-well chamber slide (Falcon) were fixed with 4% paraformaldehyde and permeabilized with 0.25% Triton X-100. The cell monolayer was then incubated with rabbit anti-IRF-1 antibody (1:50 dilution, catalogue no. 8478; Cell Signaling Technology) at 4 °C overnight, followed by a secondary antibody, goat anti-rabbit Alexa Fluor 488 (1:200 dilution, Thermo Fisher Scientific). Nuclei were counterstained with 4,6-diamidino-2-phenylindole (DAPI). Images were collected using a Leica DMIRB Inverted Microscope at UNC Michael Hooker Microscopy Facility.

Statistical analysis. Unless noted otherwise, all between-group comparisons were carried out using analysis of variance (ANOVA) or Student's *t*-test using the Prism 6.0 software (GraphPad Software). The *P* values were calculated from three biological replicates unless otherwise indicated. In some experiments designed to validate earlier conclusions using orthogonal approaches, we carried out two independent experiments, each with three technical replicates. These few exceptions are noted in the legends.

Reporting Summary. Further information on research design is available in the Nature Research Reporting Summary linked to this article.

Data availability

All data supporting the findings of this study are available within the paper and in its Supplementary Information. The RNA-seq data have been deposited with the Gene Expression Omnibus (GSE114916).

Received: 15 January 2019; Accepted: 6 March 2019;
Published online: 15 April 2019

References

1. Yoneyama, M., Onomoto, K., Jogi, M., Akaboshi, T. & Fujita, T. Viral RNA detection by RIG-I-like receptors. *Curr. Opin. Immunol.* **32**, 48–53 (2015).
2. Chan, Y. K. & Gack, M. U. Viral evasion of intracellular DNA and RNA sensing. *Nat. Rev. Microbiol.* **14**, 360–373 (2016).
3. Li, K., Chen, Z., Kato, N., Gale, M. Jr. & Lemon, S. M. Distinct poly(I-C) and virus-activated signaling pathways leading to interferon-β production in hepatocytes. *J. Biol. Chem.* **280**, 16739–16747 (2005).
4. Woodson, S. E. & Holbrook, M. R. Infection of hepatocytes with 17-D vaccine-strain yellow fever virus induces a strong pro-inflammatory host response. *J. Gen. Virol.* **92**, 2262–2271 (2011).
5. Feng, H. et al. NLRX1 promotes immediate IRF1-directed antiviral responses by limiting dsRNA-activated translational inhibition mediated by PKR. *Nat. Immunol.* **18**, 1299–1309 (2017).
6. Lemon, S. M., Ott, J. J., Van Damme, P. & Shouval, D. Type A viral hepatitis: a summary and update on the molecular virology, epidemiology, pathogenesis and prevention. *J. Hepatol.* **68**, 167–184 (2018).
7. Hirai-Yuki, A. et al. MAVS-dependent host species range and pathogenicity of human hepatitis A virus. *Science* **353**, 1541–1545 (2016).
8. Taki, S. et al. Multistage regulation of Th1-type immune responses by the transcription factor IRF-1. *Immunity* **6**, 673–679 (1997).
9. White, L. C. et al. Regulation of *LMP2* and *TAP1* genes by IRF-1 explains the paucity of CD8$^+$T cells in IRF-1$^{-/-}$mice. *Immunity* **5**, 365–376 (1996).
10. Fujita, T., Kimura, Y., Miyamoto, M., Barsoumian, E. L. & Taniguchi, T. Induction of endogenous IFN-α and IFN-β genes by a regulatory transcription factor, IRF-1. *Nature* **337**, 270–272 (1989).
11. Odendall, C. et al. Diverse intracellular pathogens activate type III interferon expression from peroxisomes. *Nat. Immunol.* **15**, 717–726 (2014).
12. Schoggins, J. W. et al. A diverse range of gene products are effectors of the type I interferon antiviral response. *Nature* **472**, 481–485 (2011).
13. Dixit, E. et al. Peroxisomes are signaling platforms for antiviral innate immunity. *Cell* **141**, 668–681 (2010).
14. Sumpter, R.Jr et al. Regulating intracellular antiviral defense and permissiveness to hepatitis C virus RNA replication through a cellular RNA helicase, RIG-I. *J. Virol.* **79**, 2689–2699 (2005).
15. Leblanc, J. F., Cohen, L., Rodrigues, M. & Hiscott, J. Synergism between distinct enhanson domains in viral induction of the human beta interferon gene. *Mol. Cell. Biol.* **10**, 3987–3993 (1990).
16. Miyamoto, M. et al. Regulated expression of a gene encoding a nuclear factor, IRF-1, that specifically binds to IFN-β gene regulatory elements. *Cell* **54**, 903–913 (1988).
17. Tanaka, N., Kawakami, T. & Taniguchi, T. Recognition DNA sequences of interferon regulatory factor 1 (IRF-1) and IRF-2, regulators of cell growth and the interferon system. *Mol. Cell. Biol.* **13**, 4531–4538 (1993).
18. Oikawa, T. et al. Model of fibrolamellar hepatocellular carcinomas reveals striking enrichment in cancer stem cells. *Nat. Commun.* **6**, 8070 (2015).
19. Uyama, T., Jin, X. H., Tsuboi, K., Tonai, T. & Ueda, N. Characterization of the human tumor suppressors TIG3 and HRASLS2 as phospholipid-metabolizing enzymes. *Biochim. Biophys. Acta* **1791**, 1114–1124 (2009).
20. Staring, J. et al. PLA2G16 represents a switch between entry and clearance of Picornaviridae. *Nature* **541**, 412–416 (2017).

21. Hsu, T. H. et al. Involvement of RARRES3 in the regulation of Wnt proteins acylation and signaling activities in human breast cancer cells. *Cell Death Differ.* **22**, 801–814 (2015).
22. Ou, C. C. et al. Downregulation of HER2 by RIG1 involves the PI3K/Akt pathway in ovarian cancer cells. *Carcinogenesis* **29**, 299–306 (2008).
23. Chiang, G. G. & Abraham, R. T. Phosphorylation of mammalian target of rapamycin (mTOR) at Ser-2448 is mediated by p70S6 kinase. *J. Biol. Chem.* **280**, 25485–25490 (2005).
24. Figueiredo, V. C., Markworth, J. F. & Cameron-Smith, D. Considerations on mTOR regulation at serine 2448: implications for muscle metabolism studies. *Cell. Mol. Life Sci.* **74**, 2537–2545 (2017).
25. Wang, J. et al. Negative regulation of Nmi on virus-triggered type I IFN production by targeting IRF7. *J. Immunol.* **191**, 3393–3399 (2013).
26. McCarthy, M. K. & Weinberg, J. B. The immunoproteasome and viral infection: a complex regulator of inflammation. *Front. Microbiol.* **6**, 21 (2015).
27. Verweij, M. C. et al. Viral inhibition of the transporter associated with antigen processing (TAP): a striking example of functional convergent evolution. *PLoS Pathog.* **11**, e1004743 (2015).
28. Schoggins, J. W. et al. Pan-viral specificity of IFN-induced genes reveals new roles for cGAS in innate immunity. *Nature* **505**, 691–695 (2014).
29. Langlais, D., Barreiro, L. B. & Gros, P. The macrophage IRF8/IRF1 regulome is required for protection against infections and is associated with chronic inflammation. *J. Exp. Med.* **213**, 585–603 (2016).
30. Nair, S., Poddar, S., Shimak, R. M. & Diamond, M. S. Interferon regulatory factor-1 (IRF-1) protects against chikungunya virus induced immunopathology by restricting infection in muscle cells. *J. Virol.* **91**, e01419-17 (2017).
31. Dansako, H. et al. Class A scavenger receptor 1 (MSR1) restricts hepatitis C virus replication by mediating toll-like receptor 3 recognition of viral RNAs produced in neighboring cells. *PLoS Pathog.* **9**, e1003345 (2013).
32. Yamane, D. et al. Regulation of the hepatitis C virus RNA replicase by endogenous lipid peroxidation. *Nat. Med.* **20**, 927–935 (2014).
33. Yamane, D. et al. Differential hepatitis C virus RNA target site selection and host factor activities of naturally occurring miR-122 3′ variants. *Nucleic Acids Res.* **45**, 4743–4755 (2017).
34. Feng, Z. et al. A pathogenic picornavirus acquires an envelope by hijacking cellular membranes. *Nature* **496**, 367–371 (2013).
35. Hishiki, T. et al. Interferon-mediated ISG15 conjugation restricts dengue virus 2 replication. *Biochem. Bioph. Res. Co.* **448**, 95–100 (2014).
36. Beard, M. R., Cohen, L., Lemon, S. M. & Martin, A. Characterization of recombinant hepatitis A virus genomes containing exogenous sequences at the 2A/2B junction. *J. Virol.* **75**, 1414–1426 (2001).
37. Binn, L. N. et al. Primary isolation and serial passage of hepatitis A virus strains in primate cell cultures. *J. Clin. Microbiol.* **20**, 28–33 (1984).
38. Matsuda, M. et al. High-throughput neutralization assay for multiple flaviviruses based on single-round infectious particles using dengue virus type 1 reporter replicon. *Sci. Rep.* **8**, 16624 (2018).
39. Yi, M. & Lemon, S. M. Replication of subgenomic hepatitis A virus RNAs expressing firefly luciferase is enhanced by mutations associated with adaptation of virus to growth in cultured cells. *J. Virol.* **76**, 1171–1180 (2002).
40. Baba, T. et al. Phosphatidic acid (PA)-preferring phospholipase A1 regulates mitochondrial dynamics. *J. Biol. Chem.* **289**, 11497–11511 (2014).
41. Imae, R. et al. LYCAT, a homologue of *C. elegans* acl-8, acl-9, and acl-10, determines the fatty acid composition of phosphatidylinositol in mice. *J. Lipid Res.* **53**, 335–347 (2012).
42. Kielkowska, A. et al. A new approach to measuring phosphoinositides in cells by mass spectrometry. *Adv. Biol. Regul.* **54**, 131–141 (2014).
43. Dobin, A. et al. STAR: ultrafast universal RNA-seq aligner. *Bioinformatics* **29**, 15–21 (2013).
44. Patro, R., Duggal, G., Love, M. I., Irizarry, R. A. & Kingsford, C. Salmon provides fast and bias-aware quantification of transcript expression. *Nat. Methods* **14**, 417–419 (2017).
45. Love, M. I., Huber, W. & Anders, S. Moderated estimation of fold change and dispersion for RNA-seq data with DESeq2. *Genome Biol.* **15**, 550 (2014).

Acknowledgements

The authors thank C.M. Rice, S. Inoue and N. Kato for the reagents, M. Soloway for the bioinformatics support, M. Chua for technical assistance and H. Dansako, B.B. Queliconi and W.J. Zuercher for helpful discussions. This work was supported in part by the Japan Society for the Promotion of Science (JSPS KAKENHI) (grant nos. JP16H07462 and JP17H05070 to D.Y., grant no. JP18K05987 to A.H-Y., grant no. JP17K08870 and JP15K19109 to T.H.), Japan Agency for Medical Research and Development (grant no. JP18jk0210014 to A.H.-Y., grant no. JP18fk0108035 to T.H. and grant no. JP16fk0210108 to M.K.) and National Institutes of Health grant no. R01-AI103083 and U19-AI109965 to S.M.L. and grant no. R01-AI131685 to S.M.L. and J.K.W.

Author contributions

D.Y. and S.M.L. conceived the study and wrote the manuscript. D.Y., H.F., E.E.R.-S., A.H.-Y., K.L.M., I.M., L.H., W.L. and O.G.-L. performed the experiments. S.R.S. and P.S. performed the bioinformatics analysis. H.N. and T.O.-N. performed the lipidomics analysis. A.D., R.S., M.M., T.H., E.W., T.O., K.M., L.M.R., M.K. and J.K.W. provided the research materials and supervised the experiments. All authors commented on the manuscript.

Competing interests

The authors declare no competing interests.

Additional information

Supplementary information is available for this paper at https://doi.org/10.1038/s41564-019-0425-6.

Reprints and permissions information is available at www.nature.com/reprints.

Correspondence and requests for materials should be addressed to D.Y. or S.M.L.

Publisher's note: Springer Nature remains neutral with regard to jurisdictional claims in published maps and institutional affiliations.

nature research

Corresponding author(s): Stanley M. Lemon and Daisuke Yamane

Reporting Summary

Nature Research wishes to improve the reproducibility of the work that we publish. This form provides structure for consistency and transparency in reporting. For further information on Nature Research policies, see Authors & Referees and the Editorial Policy Checklist.

Statistical parameters

When statistical analyses are reported, confirm that the following items are present in the relevant location (e.g. figure legend, table legend, main text, or Methods section).

n/a	Confirmed
☐	☒ The exact sample size (*n*) for each experimental group/condition, given as a discrete number and unit of measurement
☐	☒ An indication of whether measurements were taken from distinct samples or whether the same sample was measured repeatedly
☐	☒ The statistical test(s) used AND whether they are one- or two-sided *Only common tests should be described solely by name; describe more complex techniques in the Methods section.*
☐	☒ A description of all covariates tested
☐	☒ A description of any assumptions or corrections, such as tests of normality and adjustment for multiple comparisons
☐	☒ A full description of the statistics including central tendency (e.g. means) or other basic estimates (e.g. regression coefficient) AND variation (e.g. standard deviation) or associated estimates of uncertainty (e.g. confidence intervals)
☐	☒ For null hypothesis testing, the test statistic (e.g. *F*, *t*, *r*) with confidence intervals, effect sizes, degrees of freedom and *P* value noted *Give P values as exact values whenever suitable.*
☒	☐ For Bayesian analysis, information on the choice of priors and Markov chain Monte Carlo settings
☒	☐ For hierarchical and complex designs, identification of the appropriate level for tests and full reporting of outcomes
☐	☒ Estimates of effect sizes (e.g. Cohen's *d*, Pearson's *r*), indicating how they were calculated
☐	☒ Clearly defined error bars *State explicitly what error bars represent (e.g. SD, SE, CI)*

Our web collection on statistics for biologists may be useful.

Software and code

Policy information about availability of computer code

Data collection	RNA-sequencing was aligned to hg38 using STAR v2.4.2a42, genes were quantified using SalmonBeta-0.4.243, and differential expression was determined using DESeq244. Immunoblots were visualized using Odyssey Infrared Imaging System (LI-COR). Luciferase assays were carried out using Synergy 2 (Bio-Tek) or Mithras LB 940 (Berthold).
Data analysis	Gene ontology enrichment analysis was performed using DAVID 6.8. All between-group comparisons were carried out by ANOVA or t test using Prism 6.0 software (GraphPad Software, Inc.). Immunoblot bands were quantified using Image Studio 3.1.4 (LI-COR).

For manuscripts utilizing custom algorithms or software that are central to the research but not yet described in published literature, software must be made available to editors/reviewers upon request. We strongly encourage code deposition in a community repository (e.g. GitHub). See the Nature Research guidelines for submitting code & software for further information.

Data

Policy information about availability of data

All manuscripts must include a data availability statement. This statement should provide the following information, where applicable:

- Accession codes, unique identifiers, or web links for publicly available datasets
- A list of figures that have associated raw data
- A description of any restrictions on data availability

All data supporting the findings of this study are available within the paper and its Supplementary Information. RNA-sequencing data has been deposited with GEO (GSE114916).

Field-specific reporting

Please select the best fit for your research. If you are not sure, read the appropriate sections before making your selection.

☒ Life sciences ☐ Behavioural & social sciences ☐ Ecological, evolutionary & environmental sciences

For a reference copy of the document with all sections, see nature.com/authors/policies/ReportingSummary-flat.pdf

Life sciences study design

All studies must disclose on these points even when the disclosure is negative.

Sample size	We show data from 3 biological replicates from which the p values were calculated unless otherwise indicated. In some experiments designed to validate earlier conclusions using orthogonal approaches, we carried out 2 independent experiments, each with 3 technical replicates. These few exceptions are noted in the manuscript. Also, fecal shedding of HAV from mice shown in Fig. 1c is compared across the two groups (WT vs. Irf1-/-) of 4 animals in each, combining data from both day 5 and day 7 samples (8 samples from each group), as mentioned in the figure legend.
Data exclusions	No data were excluded.
Replication	All attempts at replication were successful.
Randomization	Randomization is not relevant to our study as viral infections or transfections of cells examine the response of entire cell populations.
Blinding	Investigators were not blinded during experiments. Data reported are not subjective but rather based on quantitative RT-PCR, focus forming assay, or luciferase assays.

Reporting for specific materials, systems and methods

Materials & experimental systems

n/a	Involved in the study
☒	☐ Unique biological materials
☐	☒ Antibodies
☐	☒ Eukaryotic cell lines
☒	☐ Palaeontology
☐	☒ Animals and other organisms
☒	☐ Human research participants

Methods

n/a	Involved in the study
☒	☐ ChIP-seq
☒	☐ Flow cytometry
☒	☐ MRI-based neuroimaging

Antibodies

Antibodies used	IRF1 (#8478), IRF7 (#13014), IFIT1 (#14769), STAT1 (#14994), STING (#13647), MyD88 (#4283), TLR3 (#6961), NF-kB p65 (RelA; #8242), mTOR (#2983), phospho-mTOR (Ser-2448) (#5536), phospho-mTOR (Ser-2481) (#2974), p70S6K (#2708), phospho-p70S6K (Thr-389) (#9234), 4E-BP1 (#9644) and phospho-4E-BP1 (Thr-70) (#9455) were from Cell Signaling Technology; IRF3 (sc-9082) and OAS1 (F-3, sc-374656) were from Santa Cruz Biotechnology; LGP2 (ab67270) was from Abcam; GAPDH was from Thermo Fisher Scientific (Clone 6C5; AM4300) or Wako (Clone 5A12; 016-25523); RIG-I (Clone Alme-1; ALX-804-849), Cardif (MAVS; ALX-210-929) and MDA5 (ALX-210-935-C100) were from Enzo life sciences; Actin (Clone AC-74; A2228), alpha-tubulin (Clone DM1A; T6199) and , IL28RA (AV48070) were from Sigma; IFNAR1 (A304-290A) and NMI (A300-551A) were from Bethyl

	Laboratories; and LMP2 (PSMB9; 14544-1-AP), APOL1 (11486-AP) and RARRES3 (12065-1-AP) were from Proteintech. IRDye 680 or 800 secondary antibodies including #926-32211, #926-32212, #926-32214, #926-68020 and #926-68073 were from LI-COR.
Validation	Antibodies have been published previously. Antibodies to host factors linked to antiviral signaling are validated by siRNA/shRNA knockdown or CRISPR/Cas9 knockout approaches to confirm the specificity. Interferon stimulated gene proteins were validated by stimulation with recombinant interferons.

Eukaryotic cell lines

Policy information about cell lines

Cell line source(s)	PH5CH8 cells were obtained from Dr. Nobuyuki Kato at Okayama University (Okayama, Japan). Huh-7.5 cells and 293FT cells were from Apath LLC (Brooklyn, New York, USA) and Invitrogen (Carlsbad, CA, USA), respectively.
Authentication	Microscopic inspection to validate the morphology. Huh-7.5 cells were confirmed to lack RIG-I-dependent responses through stimulation with Sendai virus challenge.
Mycoplasma contamination	All cell lines were tested negative for mycoplasma contamination using a commercial kit. Primary cells were not tested.
Commonly misidentified lines (See ICLAC register)	N/A.

Animals and other organisms

Policy information about studies involving animals; ARRIVE guidelines recommended for reporting animal research

Laboratory animals	Irf1-/-, Irf3-/- and Ifnar1-/- animals at 6-10 weeks of age on the C57Bl/6 genetic background (The Jackson Laboratory, Bar Harbor, ME, U.S.A.) C57Bl/6 animals as control.
Wild animals	The study did not involve wild animals.
Field-collected samples	The study did not involve samples collected from the field.